




# Bionic Design to Reduce Driving Power for a Portable Elbow Exoskeleton Based on Gravity-balancing Coupled Model

Qiaoling Meng<sup>1,2</sup> · Rongna Xu<sup>1,2</sup> · Qiaolian Xie<sup>1,2</sup> · Bostan-Mahmutjan<sup>1,2</sup> · Sujiao Li<sup>1,2</sup> · Hongliu Yu<sup>1,2</sup> 

Received: 12 April 2022 / Revised: 17 July 2022 / Accepted: 20 July 2022 / Published online: 29 August 2022  
© Jilin University 2022

## Abstract

Portability is an important performance to the design of exoskeleton for rehabilitation and assistance. However, the structure of traditional exoskeletons will decrease the portability because of their heavy weight and large volume. This paper proposes a novel bionic portable elbow exoskeleton based on a human-exoskeleton gravity-balancing coupled model. The variable stiffness characteristics of the coupled model is analyzed based on the static analysis. In addition, the optimization of human-exoskeleton joint points is analysis to improve the bionic motor characteristics of the exoskeleton. Theoretical prototype is designed and its driving power and dynamic performance are analyzed. Then, a prototype is designed and manufactured with a total weight of 375 g. The merits of driving power reducing is verified by simulation and the isokinetic experiments. The simulation and isokinetic results show that the driving torque and the driving power of the subject were significantly decreased with wearing the proposed exoskeleton. The driving torques are reduced 79.28% and 57.38% from the simulation results and isokinetic experiment results, respectively. The driving work of experiment was reduced by 56.5%. The development of the novel elbow exoskeleton with gravity-balancing mechanism can expand the application of exoskeleton in home-based rehabilitation.

**Keywords** Elbow exoskeleton · Bionic · Gravity-balancing · Human-exoskeleton coupled model · Portability

## 1 Introduction

Stroke is one of the diseases that cause the dysfunction of limbs according to WHO report [1]. Approximately 60–80% of stroke survivors have residual limb dysfunction at varying levels. The most frequent aftereffects are upper limb dysfunction, including muscle weakness and limited range of motion (ROM) of joints [2, 3]. The function of the upper limb can be improved by long-term and repeated rehabilitation training. However, traditional rehabilitation robots can only provide a period of rehabilitation training in hospitals. The rehabilitation plan could be interrupted for several reasons by the patient [4–7]. Exoskeleton robots have been

inspired by many researchers' attention due to their potential wearability and portability [8, 9], which could provide home-based rehabilitation training to avoid the aforementioned problem.

In the earlier research, most exoskeletons were designed based on rigid transmission mechanism, such as gear, linkage, and belts, driven by motors or hydraulic actuators [10]. This type of exoskeleton can provide precise and reliable motion. For instance, Co-Exos robot [11], ARMin [12], NESM [13], RUPERT [14]. The typical design method for this type of rigid exoskeleton places the motors/actuators at the joints' position to provide power directly. Even if their wearability is increased, such design can increase the total weight and volume of the robots. Therefore, the type of exoskeleton was commonly designed as a fixed rehabilitation robot that was utilized in hospitals. The portability of this type of exoskeleton is limited because of the mechanism design method. With the development of soft exoskeleton technology, researchers began to induce the technology into rehabilitation robots due to their structure characteristics of light-weight, compliance, and simple transmission

✉ Hongliu Yu  
yhl\_usst@outlook.com

<sup>1</sup> Institute of Rehabilitation Engineering and Technology, University of Shanghai for Science and Technology, No. 516, Jungong Road, Yangpu District, Shanghai 200093, China

<sup>2</sup> Shanghai Engineering Research Center of Assistive Devices, Shanghai 200093, China

mechanism. These merits of the soft exoskeleton improve the portability of the traditional rigid exoskeleton.

Soft exoskeleton is a type of compliant mechanism that transfers force/moment and motion through soft materials such as cable [15–17], spring [18], and composite structure material [19–22]. This type of exoskeleton uses the human limbs as manipulators, and the compliant transmission mechanism drives human limbs directly. As for the design of cable-driven exoskeleton, it has high portability but poor power transfer efficiency because the muscles of loaded limbs will absorb part of the energy during the motion [23]. The design of compliant exoskeleton with springs and composite structure material has power transfer efficiency but a lower force-weight ratio [24, 25]. Meanwhile, soft exoskeleton robots also need to overcome the weight of human limbs as well as the stiffness of the body's joints during the actuation process, which generates a large amount of power consumption. Usually, the two types of exoskeleton need more power actuators, such as hydraulic actuators. Such this, even the mechanisms are light and portable at the human limb, the portability is still weak because of the high weight and volume of their power actuators. Especially, the portability of the upper limb exoskeleton will be more limited due to the characteristics of the upper limb movement chain. Meanwhile, the portability can be improved by losing enough driving power. If introducing the concept of gravity balancing into the design of soft exoskeleton robots could significantly reduce the inertial and energy consumption of the device.

At present, many researchers have designed exoskeleton robots based on gravity balance mechanism [26–28]. For example, Wu Qingcong et al. [29, 30] developed a fixed upper limb rehabilitation exoskeleton robot system with gravity balance characteristics. The sEMG activities experiment showed that they were reduced 43% with the proposed balance mechanism. However, the gravity-balancing device used zero-free-length springs and auxiliary parallel linkages to locate the center of mass of the exoskeleton to keep the total potential energy of the system. Marcus Puchinger et al. Proposed a RETRAINER exoskeleton based on wheelchair to solve the mobility of the upper limb rehabilitation robot [31]. They also designed a passive gravity compensation mechanism mounted on a wheelchair for the proposed exoskeleton to solve the stability of the total system. The pre-tensioned spring and alignment device (combined with rope and pulley) were fixed in shoulder module to provide gravity compensation for the shoulder joint. It can only provide partial compensation with the change of the shoulder joint angle. These type of upper limb rehabilitation exoskeleton with gravity-balancing mechanism can effectively reduce

driving force, but they have poor portability due to their high weight and volume. To improve the portability, Dong et al. proposed a light-weight upper limb exoskeleton named H-VEX based on an energy-storage multi-linkage mechanism [32]. This multi-linkage mechanism can dissipate energy of spring with the increase of the wearer's shoulder joint angle. The sEMG activities experiment verified that there was significant reduction in muscle activation. However, the gravity-balancing mechanism has constant stiffness that can affect the human–exoskeleton interaction. In addition, the control strategy of the exoskeleton with the gravity-balancing mechanism will be complicated because of the nonlinear stiffness characteristics during the movement. There is a lot of research on the control algorithms of the exoskeletons. For instance, Mostafa Taghizadeh et al. proposed a series of control optimization algorithms to improve the robustness and dynamic performance of the exoskeleton control [33–35]. The dynamic performance of an exoskeleton without gravity-balancing mechanism will be changed due to the joint stiffness variation. Thus, the control robustness can be influenced. As mentioned above, adding a gravity-balancing mechanism to the exoskeleton is an effective method for decreasing the power of the system. However, gravity-balancing mechanism with constant stiffness cannot improve the portability, comfortability and the robustness because of the nonlinear joint stiffness characteristics during the movement. In addition, the human arm and exoskeleton coupled model can increase the nonlinear characteristics due to the synergic movement of the muscle and exoskeleton.

Therefore, the target of this paper is to improve the portability, the optimization of driving power and human–exoskeleton interaction in the design of a wearable exoskeleton. The major contributions of this work are as follows. This paper proposes and analyzes a human-exoskeleton coupled gravity-balancing model. Meanwhile, a novel bionic elbow exoskeleton with the gravity-balancing mechanism is also designed in this work based on the coupled model. We first finish the fully detailed analysis of the stiffness characteristic of the proposed human-exoskeleton coupled gravity-balancing model, including the optimal method of the human-exoskeleton joint point position. The theoretical prototype is designed and its dynamic performance is analyzed. Second, a novel elbow exoskeleton is designed based on the proposed model. The novel elbow exoskeleton can adapt to the stiffness variation during the elbow movement, especially the driving power can be reduced after the mechanism reaches balance. Lastly, the elbow exoskeleton performance tests are conducted after manufactured.

The rest of this paper is structured as follows. A human-exoskeleton coupled gravity-balancing model is proposed and analyzed based on its stiffness characteristics in Sect. 2. Section 3 describes the design of a light-weight wearable elbow joint exoskeleton with gravity-balancing mechanism. The driving power, working space and peak torque are analyzed to characterize its dynamic performance. Section 4 introduces the experiment of driving torque measurement and discusses the results of the experiment. Finally, the conclusion is drawn in Sect. 5.

## 2 Analysis of the Stiffness Characteristics of the Human-Exoskeleton Coupled Gravity-Balancing Model

### 2.1 Human-Exoskeleton Coupled Model

The human-exoskeleton coupled model of the upper limb exoskeleton is shown in Fig. 1. The coordinate system of the human elbow joint is defined as  $\{O\}$ , and the coordinate system of the exoskeleton on one side is defined as  $\{E\}$ , the other side is defined as  $\{E'\}$ .  $P_i (i=1, 2)$  are anchor points of elastic component of the exoskeleton in  $\{E\}$ ,  $P'_i (i=1, 2)$  are the points in  $\{E'\}$ .  $W_i (i=1, 2)$  are the points of human forearm and upper arm corresponding  $P_i$ . The desired exoskeleton in this paper is a kind of symmetrical mechanism, one side of the exoskeleton is described and analyzed for the total exoskeleton. There is a general vector offset between  $\{O\}$  and  $\{E\}$ . Therefore, this paper uses a mathematics of mapping to describe  $\{E\}$  by  $\{O\}$ . The homogenous transform can be deduced:

$$\begin{bmatrix} {}^O P_i \\ 1 \end{bmatrix} = \begin{bmatrix} {}^O R & P_{EORG} \\ 0 & 1 \end{bmatrix} \begin{bmatrix} {}^E P_i \\ 1 \end{bmatrix}, \tag{1}$$

where  $P_{EORG}$  is the position vector from  $\{E\}$  to  $\{O\}$ .  ${}^O T_E$  describe the homogeneous transforms from  $\{E\}$  relative to  $\{O\}$ , and  ${}^O R_E$  describe the rotation transforms. Where  $Q_O$  represents an original point of  $\{O\}$  placed at the revolute joint that is equivalent to the human elbow joint, and  $Q_E$  is the revolute joint of the desired exoskeleton, especially  $\theta_E$  is the rotation angle of  $\{E\}$  relative to  $\{O\}$ . In Fig. 1a, the coordinate of  $Q_E$  is  $(d, 0, 0)$  in  $\{O\}$ , where  $d$  is the translation quantity from  $Q_E$  to  $Q_O$ . The homogeneous transform matrix is obtained as:

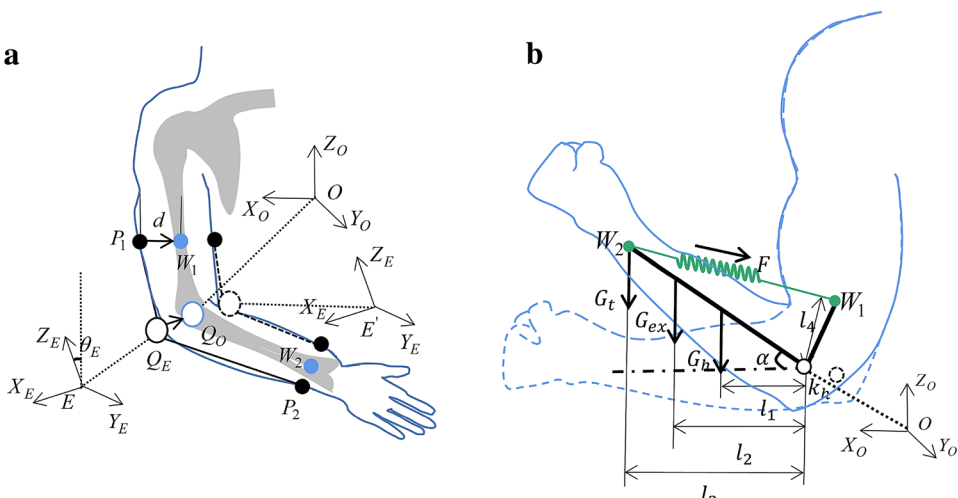
$${}^O T_E = \begin{bmatrix} \cos \theta_E & -\sin \theta_E & 0 & d \\ \sin \theta_E & \cos \theta_E & 0 & 0 \\ 0 & 0 & 1 & 0 \\ 0 & 0 & 0 & 1 \end{bmatrix}. \tag{2}$$

Combining (1) and (2), and the coordinate of  ${}^E P_i$  is  $({}^E P_{i,x}, {}^E P_{i,y}, {}^E P_{i,z})$ , the homogenous coordinate of  ${}^O P_i$  is:

$$\begin{bmatrix} x \\ y \\ z \\ 1 \end{bmatrix} = \begin{bmatrix} \cos \theta_E & -\sin \theta_E & 0 & d \\ \sin \theta_E & \cos \theta_E & 0 & 0 \\ 0 & 0 & 1 & 0 \\ 0 & 0 & 0 & 1 \end{bmatrix} \begin{bmatrix} {}^E P_{i,x} \\ {}^E P_{i,y} \\ {}^E P_{i,z} \\ 1 \end{bmatrix}. \tag{3}$$

In addition, the points  $w_1$  and  $w_2$  are the point projection of  ${}^O p_{w,1}$  and  ${}^O p_{w,2}$  from the exoskeleton to the axes of  $OZ$  and  $OY$ , respectively. The projection transformations are defined as  $T_1$  and  $T_2$ . It is noted that the half of the thickness of human upper arm and forearm,  $t_1$  and  $t_2$ , are the element of  $T_1$  and  $T_2$  on the x-axis. Define the coordinate of  $W_i (i=1, 2)$  are  $(w_{i,x}, w_{i,y}, w_{i,z})$ . The coordinates of  ${}^O p_{w,i} (i=1, 2)$  are obtained as following:

Fig. 1 Man-machine coupled hydrostatic model. a Pre-coupled. b After-coupled



$$\begin{cases} {}^O P_{W,1} = (t_1, 0, w_{i,z}) \\ {}^O P_{W,2} = (t_2, w_{i,y}, 0) \end{cases} \quad (4)$$

Then, the points  ${}^O P_{W,i}$  to  $\{E\}$  can be deduced from (1),

$${}^E P_{W,i} = {}^O T^{-1} {}^O P_{W,i} \quad (5)$$

Combining (2) and (4), the homogenous coordinate of  ${}^E P_{W,i}$  ( $i = 1, 2$ ) is:

$$\begin{cases} {}^E P_{W,1} = \begin{bmatrix} x \\ y \\ z \\ 1 \end{bmatrix} = \begin{bmatrix} \frac{d}{\cos \theta_E} & \frac{1}{\sin \theta_E} & 0 & 0 \\ -\frac{d \sin \theta_E}{\cos^2 \theta_E} & \frac{1}{\cos \theta_E} & 0 & 0 \\ 0 & 0 & 1 & 0 \\ 0 & 0 & 0 & 1 \end{bmatrix} \begin{bmatrix} t_1 \\ 0 \\ w_{1,z} \\ 1 \end{bmatrix} \\ {}^E P_{W,2} = \begin{bmatrix} x \\ y \\ z \\ 1 \end{bmatrix} = \begin{bmatrix} \frac{d}{\cos \theta_E} & \frac{1}{\sin \theta_E} & 0 & 0 \\ -\frac{d \sin \theta_E}{\cos^2 \theta_E} & \frac{1}{\cos \theta_E} & 0 & 0 \\ 0 & 0 & 1 & 0 \\ 0 & 0 & 0 & 1 \end{bmatrix} \begin{bmatrix} t_2 \\ w_{2,y} \\ 0 \\ 1 \end{bmatrix} \end{cases} \quad (6)$$

### 2.2 Analysis of Stiffness Characteristics for the Human-Exoskeleton Coupled Model with Gravity-Balancing Mechanism

As shown in Fig. 1b, the whole force/torque of the system comprises the gravities of the human upper limb, exoskeleton and the holding objects, the interaction force between human-exoskeleton and tension of elastic component. The balancing equation can be obtained based on the principle of force balance:

$$\begin{cases} \sum {}^O M = 0 \\ \sum {}^O F_x = 0 \\ \sum {}^O F_y = 0 \end{cases} \quad (7)$$

The detailed equations can be expressed as,

$$\begin{cases} k_h \alpha + G_h l_1 \cos \alpha + G_{ex} l_2 \cos \alpha + G_t l_3 \cos \alpha = F l_4 \\ f \cos \alpha = F \sin \beta \\ f \sin \alpha + G_h + G_{ex} + G_t = F \cos \beta \end{cases}, \quad (8)$$

where  $G_h, G_{ex}, G_t$ : the gravity of forearm/exoskeleton/weight in hand;  $l_1, l_2, l_3$ : the length from the center of gravity of the forearm/exoskeleton/holding objects to the original point  $Q_O$ ;  $l_4$ : the force arm of the elastic component;  $\beta$ : the angle between  $Q_O W_2$  and  $\vec{l}_4$ . The stiffness of the human elbow is:

$$k_h = \frac{F l_4 - (G_h l_1 \cos \alpha + G_{ex} l_2 \cos \alpha + G_t l_3 \cos \alpha)}{\alpha} \quad (9-1)$$

Therefore, the force of the exoskeleton  $F$  is:

$$F = \frac{G_h + G_{ex} + G_t}{\cos \beta - \sin \beta \tan \alpha}, \quad (9-2)$$

with

$$\beta(\alpha) = \arccos \frac{{}^O p_{1,z}^2 - {}^O p_{1,z} {}^O p_{2,y} \sin \alpha}{{}^O p_{1,z} \sqrt{{}^O p_{1,z}^2 + {}^O p_{2,y}^2 - 2 {}^O p_{1,y} {}^O p_{2,y} \sin \alpha}} \quad (10)$$

The coordinate of  ${}^O P_1$  in  $\{O\}$  is  $(0, 0, {}^O p_{1,z})$  and the coordinate of  ${}^O P_2$  in  $\{O\}$  is  $(0, {}^O p_{2,y}, 0)$ .

In addition, the stiffness of exoskeleton can be described based on the parametric human-exoskeleton coupled model. This paper defines the rotational stiffness of the projection exoskeleton be  $k(\alpha)$ , the stiffness of the projection exoskeleton is established:

$$k(\alpha) = \frac{(G_h + G_{ex} + G_t) \times l_4}{(\cos \beta - \sin \beta \tan \alpha) \times \alpha} \quad (11)$$

Combining (5) and (6), the stiffness of unilateral elastic component  $k_E(\alpha)$ :

$$k_E(\alpha) = \frac{(G_h + G_{ex} + G_t) \times \sqrt{[({}^E p_{W,1,z} + {}^E p_{W,2,y})^2 - {}^E p_{W,1,z} {}^E p_{W,2,y}^2] [{}^E p_{W,1}^E p_{W,2}^2 - ({}^E p_{W,1,z} - {}^E p_{W,2,y})^2]}}{\sqrt{2} \sin(\beta(\alpha) - \alpha) \times \alpha \times {}^E p_{W,1} {}^E p_{W,2}} \quad (12)$$

where the stiffness of the other side of the exoskeleton  $k_E(\alpha)$  is equal to  $k_E(\alpha)$ .

Figure 2 shows that the stiffness curve of mechanism changes non-linearly at the first 30%, and it tends to become a constant value at the last 70%. The parameters of the elastic component have been designed according to the human-exoskeleton coupled model. This paper fits the last 70% of the stiffness as elastic component, which has a constant stiffness. The variable stiffness module has been designed to change the stiffness of the elastic component at the first 30% of the exoskeleton movement, and the module could change the length of the elastic component. Meanwhile, the relationship between the varying length of elastic component and the flexion angle of elbow joint can be obtained according to the human-exoskeleton coupled model and the stiffness parameters of the elastic component as shown in Fig. 3.

### 2.3 Optimization of Human-Exoskeleton Joint Point

The driving power can be directly effected by the moment produced by the elastic component. Optimizing the positions of the anchor points of the elastic component can utilize its output moment effectively as well as reduce the whole volume of the exoskeleton. The range of anchor points is  $0 \text{ mm} \leq x \leq 22 \text{ mm}$  [the distance from upper arm/forearm to the olecranon of the elbow (the protrusion at the back of the elbow joint, which can be reached when the elbow is flexed)]. The simulation calculates the required driving torque of different anchor point positions. As shown in Table 1, the force of the elastic component in different anchor point positions are compared in elbow flexion angles from  $0^\circ$  to  $45^\circ$ . Suppose that  $w_{1,z} = c_1 \times l_3$  and  $w_{2,y} = c_2 \times l_3$ . Table 1 shows that most of minimal force of different angles occur in  $c_1 = 0.9$  and  $c_2 = 1.09$ . Therefore,  $w_1(0, 0, 0.9l_3)$  and  $w_2(0, 1.09l_3, 0)$  are optimal anchor points, which could ensure the minimum force required in the movement. Combining (6), the coordinates of  ${}^E p_{W,i}$  is:

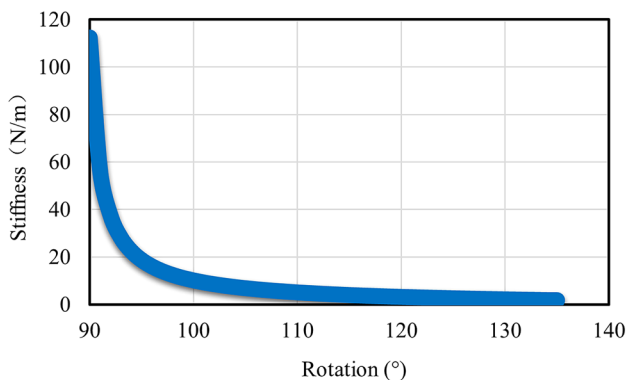


Fig. 2 Stiffness variation curves for balancing mechanisms

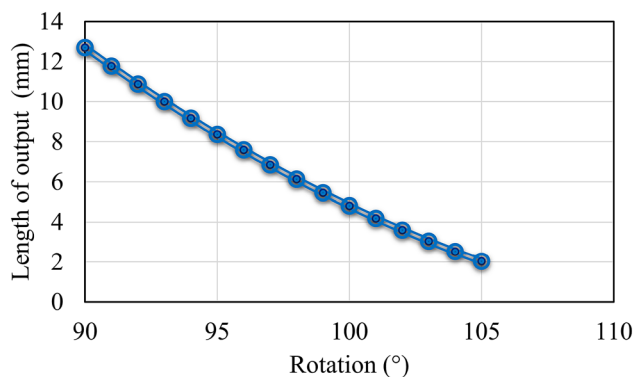


Fig. 3 Output displacement of the mechanism in relation to angle

$$\begin{cases} {}^E p_{W,1} = \left( \frac{dt_1}{\cos \theta_E}, -\frac{dt_1 \sin \theta_E}{\cos^2 \theta_E}, 0.9l_3 \right) \\ {}^E p_{W,2} = \left( \frac{dt_2}{\cos \theta_E} + \frac{1.09l_3}{\sin \theta_E}, -\frac{dt_2 \sin \theta_E}{\cos^2 \theta_E} + \frac{1.09l_3}{\cos \theta_E}, 0 \right) \end{cases} \quad (13-1)$$

The coordinates of  ${}^E p_{W,i}$  in  $\{E'\}$  are deduced by the following:

$$\begin{cases} {}^{E'} p_{W,1} = \left( -\frac{dt_1}{\cos \theta_E}, -\frac{dt_1 \sin \theta_E}{\cos^2 \theta_E}, 0.9l_3 \right) \\ {}^{E'} p_{W,2} = \left( -\frac{dt_2}{\cos \theta_E} - \frac{1.09l_3}{\sin \theta_E}, -\frac{dt_2 \sin \theta_E}{\cos^2 \theta_E} + \frac{1.09l_3}{\cos \theta_E}, 0 \right) \end{cases} \quad (13-2)$$

Therefore, the optimization results can be used to define the positions of human-exoskeleton joint points in the later exoskeleton design.

Table 1 Comparative analysis of driving forces at different anchor positions and different angles

Rotation ( $^\circ$ )	Force (N)	$c_1$	$c_2$
90	14.25	0.9	1.09
95	13.63	0.8	1.09
100	13.3	0.8465	1.09
105	12.04	0.9	1.09
110	11.27	0.9	1.09
115	10.76	0.9	1.09
120	9.909	0.9	1
125	9.096	0.9	1
130	8.357	0.9	1
135	7.7	0.9	0.91

**Fig. 4** Diagram of wearing an exoskeleton in the elbow joint

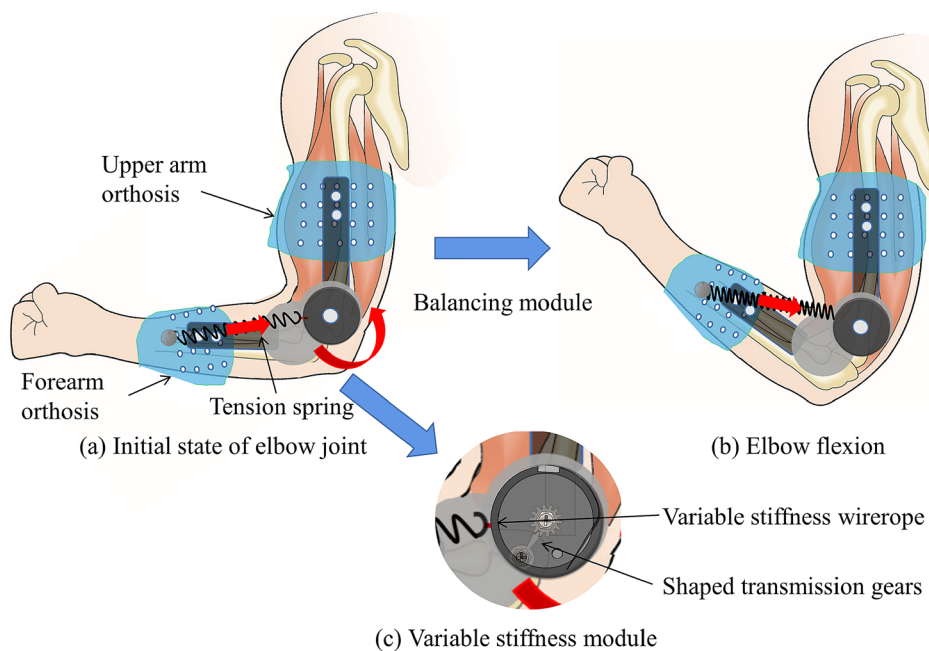
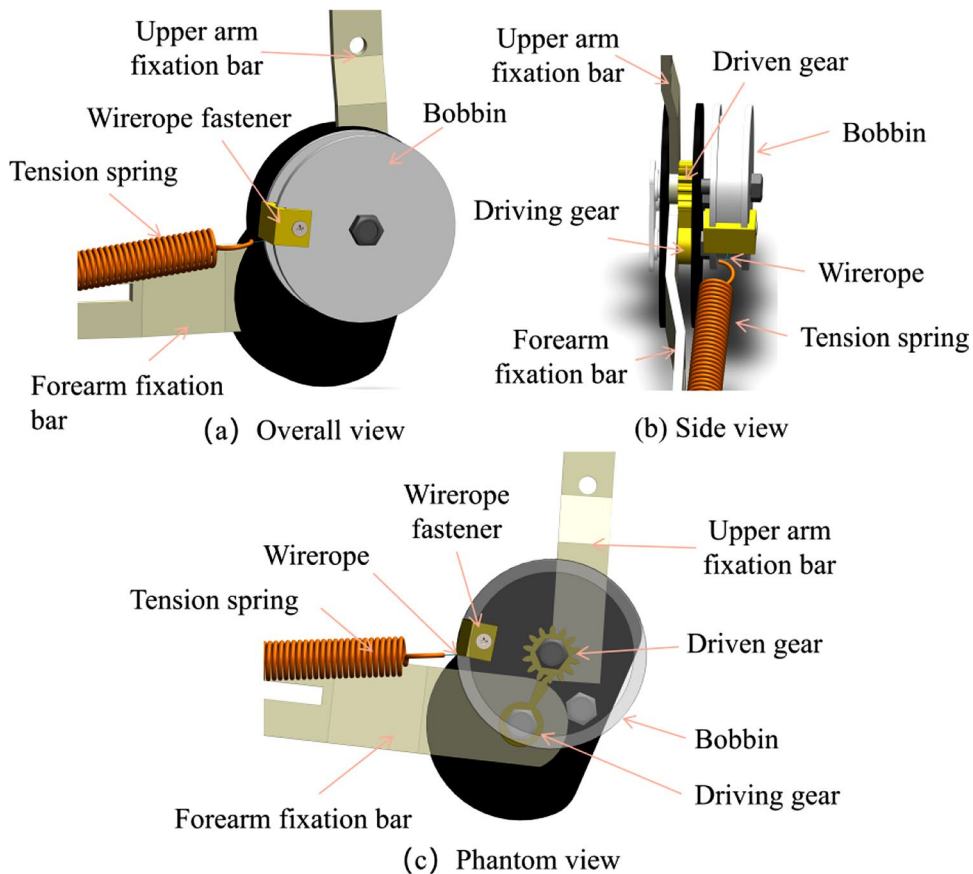


**Fig. 5** Variable stiffness models





### 3 Gravity-Balancing Elbow Exoskeleton Design

#### 3.1 The Design of Exoskeleton Mechanism

According to the characteristics of the articular surface of the elbow joint, the rotation axis of the elbow joint will change during the movement. Therefore, this paper considers the elbow joint as a bi-axial joint in the design. This paper designed a novel elbow exoskeleton with the gravity-balancing mechanism based on the human-exoskeleton coupled model as shown in Fig. 4. The exoskeleton consists of three modules: wearable module, gravity-balancing module and variable stiffness module. The wearable module is used to link the human upper limb with the gravity-balancing module and variable stiffness module, and the gravity-balancing module links with variable stiffness module. The wearable module includes upper arm orthosis and forearm orthosis to connect the human body and gravity-balancing mechanism, and the arm orthoses are fixed to the human body through elastic straps. The gravity-balancing module consists of springs and forearm/upper arm fixation bars. The hinges are designed according to the joint position of the human humerus, ulna and radius. The forearm and upper arm fixation bars have been integrated into the hinges to make the exoskeleton move around the dual axis. The springs are chosen as the elastic components, and the fixation bars are fixed on forearm/upper arm orthoses. Meanwhile, the forearm orthosis is screwed on the front end of the springs. The variable stiffness module is composed of two wire-ropes, a pair of special-shaped drive gears and a bobbin as shown in Fig. 5. The front end of two wire-ropes are welded to the springs and their back end are screwed on the bobbin. The pair of special-shaped drive gears are integrated with forearm/upper arm fixation bars, respectively, their rotation axes are identical to the bobbin's.

The range of the elbow flexion in Activity of Daily Living (ADL) is from 5° to 145° [36]. The pose of the elbow joint subjected to maximum gravity is at the flexion of 90°. Meanwhile, the variable moment produced by the gravity is symmetrical about the pose of the elbow joint at flexion at

**Table 2** The required parameters of spring

Parameters	Meaning
$L$	Spring length
$k_s$	Elastic coefficient of spring
$F_{135^\circ}$	Spring force in 135°
$F_{90^\circ}$	Spring force in 90°
$L_{45^\circ}$	Spring length in 135°
$L_{90^\circ}$	Spring length in 90°

90°. This paper analyzes the characteristic of the gravity-balancing mechanism in the range from 90° to 135°. The position of elbow flexion at 90° is defined as the initial position in this paper. When the elbow joint is flexed from 90° to 105°, the forearm fixation bar transmits the movement to the gears and thus to the bobbin. Meanwhile, the bobbin rotates the wire-ropes to adjust the stiffness of the spring. When the elbow joint is flexed to the angle of 105°–135°, the gears are disengaged and the bobbin stops rotating so that the springs can keep their constant stiffness.

Table 2 shows the required parameters to calculate the value of spring, and the relationship between the spring length and the force is:

$$F_{90^\circ} = k_s L + F_{135^\circ}. \tag{14}$$

The further parameter of the spring can be achieved by (14) and the spring's formula.

#### 3.2 Analysis of Dynamic Performance

##### 3.2.1 Driving Power

The extra driving torque required to drive the elbow joint after balancing can be calculated based on the human-exoskeleton statics model as shown in Fig. 1. The relationship between the torque and the angular acceleration is:

$$M = I \times a. \tag{15}$$

**Table 3** Comparison of workspace between human joint and mechanism

	Human elbow joint workspace limits	Functional Arc of human Elbow joint	Reachable workspace of the mechanism	Efficient workspace of the mechanism
Flexion	0°–145°	30°–130°	0°–135°	90°–135°
Extension	0°–5°	0°	0°	0°

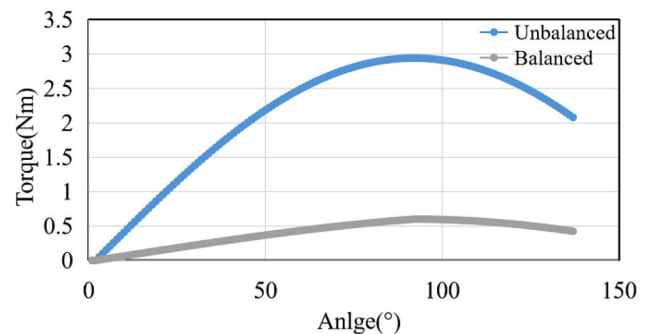


**Fig. 6** Driving torque of the reachable workspace

**Table 4** Comparison of peak torque

	Angle	Peak torque (Nm)
Unbalanced	0°–45°	2.11
	45°–90°	2.94
	90°–135°	2.94
Balanced	0°–45°	0.35
	45°–90°	0.59
	90°–135°	0.59

The detailed equations can be expressed as:

$$M = \left( m_h + m_e - \frac{F(\cos \beta - \sin \beta \tan \alpha)}{g} \right) \times \frac{(g + \mu)r^2\omega}{gt}, \tag{16}$$

where  $m_h/m_e$ : the mass of the human forearm/exoskeleton;  $r^2$ : the radius of gyration (the length of forearm);  $\omega$ : the angular velocity of elbow joint;  $\mu$  is the friction coefficient;  $t$ : the rotation time.

The quantitative description of work can evaluate whether the exoskeleton could reduce the driving power. Combining (16), the work  $W$  can be described as:

$$W = \left( m_h + m_e - \frac{F(\cos \beta - \sin \beta \tan \alpha)}{g} \right) \times \frac{(g + \mu)r^2\omega}{gt} \times \alpha. \tag{17}$$

### 3.2.2 Dynamic Characteristics

Dynamic performance describes the properties and functions of the system in the dynamic process. The dynamic performance of the mechanism proposed in this paper is mainly manifested in the movement workspace and the peak torque of each movement stage. Table 3 shows the reachable/efficient workspace of the elbow exoskeleton, the workspace limitations of the human elbow, and the functional motion

**Table 5** Values of exoskeleton prototype

Exoskeleton parameters	Value	Units
Exoskeleton weight	373	g
Forearm fixation bar length	100	mm
Upper arm fixation bar length	105	mm
Bobbin radius	25	mm
Reference diameter of driving gear	15	mm
Reference diameter of driven gear	7.5	mm

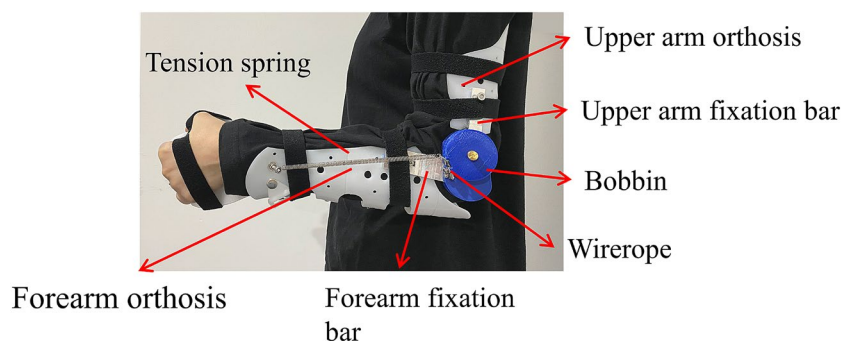
**Table 6** Spring geometry parameters

Spring parameters	Value
Initial length $s$	137.5 mm
Diameter $D$	13 mm
Wire diameter $d$	1 mm
Elasticity factor $K$	0.4 N/m

arc of the human elbow [36]. The reachable workspace of the exoskeleton is from 0° to 135°, which meets the range of movement required by the elbow for daily living activities. Therefore, the exoskeleton can assist the elbow to perform the following activities of daily living: opening the door, pouring water out of a pot, getting up from a chair, picking up a newspaper, eating and making a phone call.

Figure 6 shows the change of elbow driving torque before and after gravity balancing when the flexion angle of the elbow is from 0° to 135°. The man-mechanism coupled gravity-balancing model proposed in this paper is based on the 90°–135° of the elbow. Combined with the peak torques in different ranges in Table 4, it can be observed that the driving torque of the elbow joint of the flexion angle at 45°–90° is related to 90°–135° before and after balancing. Therefore, the elbow joint can be considered as a gravity-balancing state at 45°–135°. The exoskeleton has balanced most of the gravity and its peak torque is 17.16% of the unbalanced torque when the elbow flexes from 0° to 45°. Peak torque is 20.07% of unbalanced torque when the elbow flexes from 45° to 135°.

**Fig. 7** Exoskeleton prototype





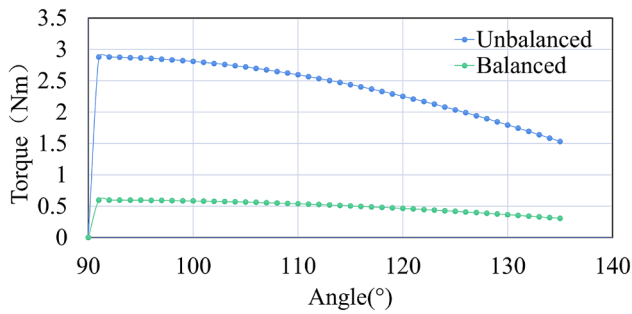


Fig. 8 The simulation results of driving torque

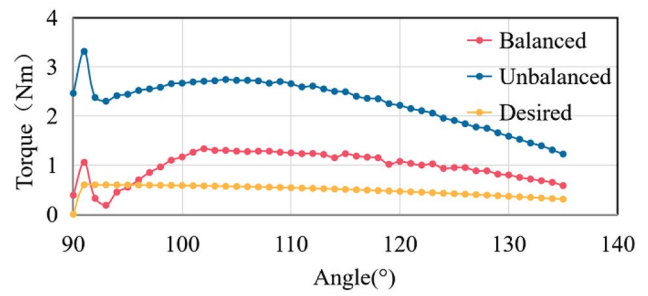


Fig. 10 Comparison of drive torque before and after balancing

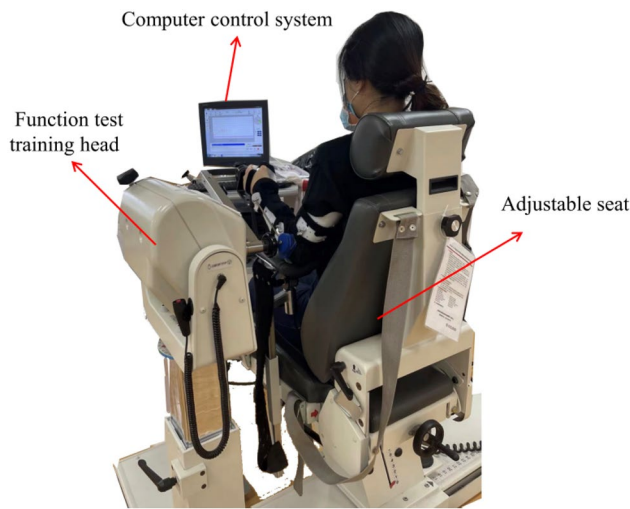


Fig. 9 The Biodex System 4

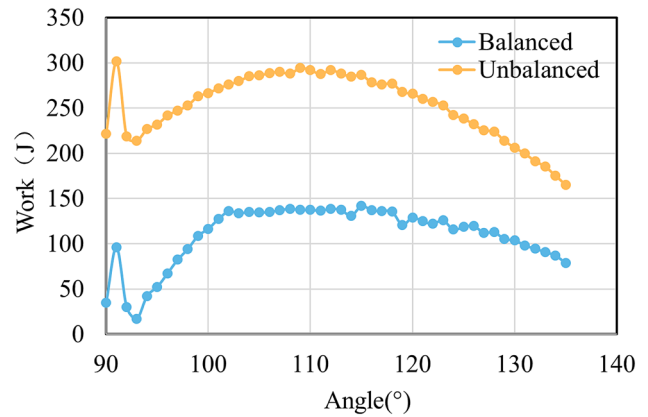


Fig. 11 Comparison of driving power before and after balancing

## 4 Prototype and Experiments

### 4.1 Prototype

The prototype was customized for a healthy volunteer (the upper arm length is 30.44 cm, the forearm length is 27.79 cm). The length and weight of each part of the human upper limb can be calculated by the value of height and weight according to the anthropometric theory [37]. The exoskeleton prototype can be designed based on the above theoretical model and human parameters as shown in Fig. 7. Table 5 shows the values of exoskeleton prototype, and the spring parameters in Table 6.

### 4.2 Simulation Experiment

The statics model is simulated to verify the effectiveness of the above human-exoskeleton coupled model and the design of the exoskeleton parameters. Suppose the angular velocity of elbow joint  $\omega = 5$  rad/min, and the coefficient

between aluminum alloy and resin friction  $\mu = 0.28$ . Combining (16), the variation trends of driving torque before and after balancing can be calculated in Fig. 8. The simulation results show that the driving moment after balancing tends to stabilize and approaches 0, and the value is lower than before wearing apparently. The simulation shows that the maximum driving torque at the flexion of  $91^\circ$  is reduced by 2.28 Nm, and the minimum driving torque at the flexion of  $135^\circ$  is reduced by 1.23 Nm. Comparing the whole errors  $\tau$  of before and after balancing, the formula can be described as following:

$$\tau = \frac{\sum_{K=90}^K M_K - \sum_{K=90}^K N_K}{\sum_{K=90}^K M_K} \times 100\%, \tag{18}$$

where  $M_K$  ( $K = 90-135$ ) are driving torque before balancing,  $N_K$  ( $K = 90-135$ ) are driving torque after balancing. The simulation results acquired by calculation show that the driving torque is reduced by 79.28% after gravity-balancing.

### 4.3 The Isokinetic Experiment

The upper limb isokinetic training system (Biodex System 4) as shown in Fig. 9 is utilized to measure the driving torque of the elbow movement. Isokinetic training is a type of rehabilitation training that applies the system to carry the human limb with a constant speed. Therefore, the driving speed of the system will not be affected by the changes of the objects' own torque.

The isokinetic training system of the upper limb is used to record the joint driving torque and elbow joint flexion angle before and after wearing the exoskeleton, and the experimental results were compared. A health volunteer (22 years old, 178 cm in height, 60 kg in weight) has been chosen for the two sets of experiments. In both sets of experiments, the elbow joint range of isokinetic training was set at 90°–135°, the training speed was 5 rad/min, and the training time was the 30 s. The subject was isokinetic training without wearing the exoskeleton. The training repeated five times and the subjects rested at intervals of 10 s. The subject took rest at intervals of 10 s and repeated training for five times under the wearing of the exoskeleton.

The relationship of torque-time and the flexion angle of Experiment Unwearing and Experiment Wearing can be obtained from the upper limb isokinetic training system. The results of experiment Unwearing and Experiment Wearing are analysis and evaluation, respectively, to obtain the relationship between the torque and the flexion angles in the process of elbow flexion.

The comparison of the two sets of experiments is shown in Fig. 10. The driving torque after wearing is significantly lower than before. The experimental result also shows that the curvature of the torque–angle is significantly lower than before balancing. The experimental results shown in Fig. 10 have been averaged to analyze the power assist effect and force balance effect of the exoskeleton quantitatively. Figure 10 shows that the maximum driving torque at the flexion of 91° is reduced by 2.06 Nm, and the minimum power at the flexion of 135° is reduced by 0.642 Nm. The driving torque and torque–angle curvature are reduced by 57.38% and 20.78% on average after wearing the exoskeleton. Figure 11 shows that the maximum power at the flexion of 110° is reduced by 154.69 J, and the minimum power at the flexion of 93° is reduced by 196.85 J. The whole driving work after balancing is reduced by 56.50%.

## 5 Discussion

The upper limb exoskeletons are widely used in rehabilitation training and have been proved to have a positive effect in restoring neurovascular injury. However, it is limited for the

**Table 7** Comparison the weights of different exoskeleton

Types	Companies	Weight (kg)
Elbow orthosis	GUANAI	0.4
	ZGONG LIANG	0.3
	Miaopu	0.3
Elbow exoskeleton with driving	ZGONG LIANG	1.18
	Dedu	2
	HUAI GU	1.18
The elbow exoskeleton with gravity-balancing	The design of this paper	0.375

traditional exoskeleton to work in a home-based rehabilitation environment due to the high weight and volume. This paper designed the light-weight elbow exoskeleton to solve the problems of portability in existing exoskeletons.

The reachable workspace of the exoskeleton proposed in this paper can be reached from 0° to 135°, which could meet requirement of the daily living activities. According to the calculation of the peak torque of 0°–135°, it can be observed that the driving torque required for elbow flexion of 45°–90° is symmetrical to 90°–135°. The peak torque of 0°–45° is reduced by 82.84% after balancing, the peak torque of 0°–45° is reduced by 79.93%.

The experiment result has a difference from the statics simulation result, which means there are some experimental errors, but these errors are under control. There are deviations between the anthropometric parameters and the actual parameters, the same as the virtual prototype and the principal prototype. A more valid revised method should be proposed to avoid this effect. The experiment of measuring the work of the driving torque in driving the elbow movement was conducted. The result shows that the driving torque and torque–angle curvature are reduced by 57.38% and 20.78% on average after wearing the exoskeleton. The work was reduced by 56.50%, which means driving power can be reduced by the gravity-balancing exoskeleton in the paper.

It can be seen from the change trend of the heavy torque that the control of the rehabilitation exoskeleton is nonlinear control, which requires a series of parameter optimization and higher precision requirements for speed and acceleration. The output torque is relatively stable after introducing the gravity-balancing mechanism, which can be regarded as linear control. The gravity-balancing mechanism can effectively reduce the complexity of exoskeleton control.

As shown in Table 7, the weight of the minimum elbow orthosis is about 300 g, and the weight of the exoskeleton in this paper is 375 g. The exoskeleton with gravity-balancing mechanism is no more than 75 g heavier than the traditional orthosis as shown in Table 7. Meanwhile, Table 7 shows that the weight of the elbow exoskeletons with extra driving power is between 1.18 and 2 kg. The weight of the proposed

elbow exoskeleton with extra power will be increased by the actuator and the transmission mechanism. It is obvious that the weight of the actuator with 1.5 Nm is less than the one with 3 Nm according to the data from the Maxon [38]. In addition, the elbow joint with exoskeleton can be driven by light-weight steering gears (the weights are about 0.02 kg) without the requirement for intelligent control. Therefore, the gravity-balancing exoskeleton has better portability even adding the extra driving power, which is beneficial to providing patients for home-based rehabilitation training.

## 6 Conclusion

This paper proposed the human-exoskeleton gravity-balancing coupled model based on analysis of its variable stiffness characteristics. On this basis, this paper also proposed the optimal design method for an elbow exoskeleton with gravity-balancing. A novel portable elbow exoskeleton with gravity-balancing mechanism was designed to reduce the driving power based on the proposed method. The theoretical prototype was designed and the dynamic performance was analyzed, which included the workspace and the peak torque. The simulation results show that in the  $0^{\circ}$ – $135^{\circ}$  exoskeleton reachable workspace, the peak torque of  $0^{\circ}$ – $45^{\circ}$  is reduced by 82.84% and the peak torque of  $0^{\circ}$ – $45^{\circ}$  is reduced by 79.93%. The prototype was manufactured and verified by the simulation and isokinetic experiments. The simulation and isokinetic results show that the driving torque and the driving power of the subject were significantly decreased with wearing the proposed exoskeleton. The output stiffness tended to be smooth. The simulation result shows that the driving torque was reduced by 79.28%, and the isokinetic experiment reduced by 57.38%. The driving work of experiment was reduced by 56.5%. The results show that the gravity-balancing method in this paper can reduce the driving power and increase the portability of the exoskeleton. In addition, the human-exoskeleton gravity-balancing coupled model and design method also can be utilized in control design of the exoskeleton.

**Acknowledgements** The authors gratefully acknowledge the financial support by National Natural Science Foundation of China (61803265, 61903255) and Shanghai Science and Technology Development Foundation, China (Grant no. 20S31905400).

**Data Availability** The datasets generated during and/or analyzed during the current study are available from the corresponding author on reasonable request.

## Declarations

**Conflict of interest** The authors declare that there is no conflict of interest.

## References

1. Mortality and global health estimates <https://www.who.int/data/gho/data/themes/mortality-and-global-health-estimates>
2. Wang, Q. X., Huang, Z., Pan, B. Y., Jin, T. T., Luo, C., & Wang, C. (2017). The biomechanics of hemiplegic stroke survivors' upper limb motor function. *Chinese Journal of Physics Medical Rehabilitation*, 39, 727–773. in Chinese.
3. Brewer, L., Horgan, F., Hickey, A., & Williams, D. (2012). Stroke rehabilitation: recent advances and future therapies. *QJM: An International Journal of Medicine*, 106, 11–25.
4. Bütefisch, C., Hummelsheim, H., Denzler, P., & Mauritz, K. H. (1995). Repetitive training of isolated movements improves the outcome of motor rehabilitation of the centrally paretic hand. *Journal of the Neurological Sciences*, 130, 59–68.
5. Charles, J., & Gordon, A. M. (2006). Development of hand–arm bimanual intensive training (HABIT) for improving bimanual coordination in children with hemiplegic cerebral palsy. *Developmental Medicine and Child Neurology*, 48, 931–936.
6. Comelia, C. L., Stebbins, G. T., Brown-Toms, N., & Goetz, C. G. (1994). Physical therapy and Parkinson's disease: A controlled clinical trial. *Neurology*, 44, 376–378.
7. Freeman, J. A., Langdon, D. W., Hobart, J. C., & Thompson, A. J. (1997). The impact of inpatient rehabilitation on progressive multiple sclerosis. *Annals of Neurology*, 42, 236–244.
8. Bianchi, M., Fanelli, F., Conti, R., Governi, L., & Allotta, B. (2017). Design and motion analysis of a wearable and portable hand exoskeleton. *In Biosystems and Biorobotics*, 16, 373–377.
9. Bongsu, K., & Ashish, D. (2017). An upper-body rehabilitation exoskeleton harmony with an anatomical shoulder mechanism: Design, modeling, control, and performance evaluation. *International Journal of Robotics Research*, 36, 414–435.
10. Rehmat, N., Jie, Z., Wei, M., Quan, L., & Hui, L. (2018). Upper limb rehabilitation using robotic exoskeleton systems: A systematic review. *International Journal of Intelligent Robotics and Applications*, 2, 5–6.
11. Zhang, L. Y., Li, J. F., Dong, M. J., Cui, Y., & Rong, X. (2019). Development of a compatible exoskeleton (Co-Exos II) for upper-limb rehabilitation\*. In *2019 16th International Conference on Ubiquitous Robots (UR)*, Jeju, Korea (pp. 240–245).
12. Nef, T., & Riener, R. (2005). ARMin—Design of a novel arm rehabilitation robot. In: *9th International conference on rehabilitation robotics*, Chicago, IL, USA (pp. 57–60).
13. Trigili, E., Crea, S., Moise, M., Baldoni, A., Cempini, M., Ercolini, G., Marconi, D., Posteraro, F., Carrozza, M. C., & Vitiello, N. (2019). Design and experimental characterization of a shoulder-elbow exoskeleton with compliant joints for post-stroke rehabilitation. *Mechatronics, IEEE/ASME Transactions on*, 2019(24), 1485–1496.
14. Jian, H., Tu, X. H., & He, J. P. (2016). Design and evaluation of the RUPERT wearable upper extremity exoskeleton robot for clinical and in-home therapies. *IEEE Transactions on Systems, Man, and Cybernetics: Systems*, 46, 1–10.
15. Cui, X., Chen, W. H., Jin, X., & Agrawal, S. K. (2017). Design of a 7-DOF cable-driven arm exoskeleton (CAREX-7) and a controller for dexterous motion training or assistance. *IEEE/ASME Transactions on Mechatronics: A Joint Publication of the IEEE*

- Industrial Electronics Society and the ASME Dynamic Systems and Control Division*, 22, 161–172.
16. Lamine, H., Laribi, M. A., Bennour, S., Romdhane, L., & Zeghloul, S. (2017). Design study of a cable-based gait training machine. *Journal of Bionic Engineering*, 14, 13.
  17. Samper-Escudero, J. L., Gimenez, A., Sanchez-Uran, M. A., & Ferre, M. (2020). A cable-driven exosuit for upper limb flexion based on fibres compliance. *IEEE Access*, 2020(99), 1–1.
  18. Higuma, T., Kiguchi, K., & Arata, J. (2017). Low-profile two-degree-of-freedom wrist exoskeleton device using multiple spring blade. *IEEE Robotics and Automation Letters*, 99, 1–1.
  19. Koh, T. H., Cheng, N., Yap, H. K., & Yeow, C. H. (2017). Design of a soft robotic elbow sleeve with passive and intent-controlled actuation. *Frontiers in Neuroscience*, 11, 597.
  20. Jiryaei, Z., Alvar, A. A., Bani, M. A., Vahedi, M., & Jafarpisheh, A. S. (2021). Development and feasibility of a soft pneumatic-robotic glove to assist impaired hand function in quadriplegia patients: A pilot study. *Journal of Bodywork and Movement Therapies*, 27, 731–736.
  21. Kai, Y. H., Hoon, L. J., & Fatima, N. (2017). Design and preliminary feasibility study of a soft robotic glove for hand function assistance in stroke survivors. *Frontiers in Neuroscience*, 11, 547.
  22. Polygerinos, P., Zheng, W., Overvelde, J., Galloway, K. C., & Walsh, C. J. (2015). Modeling of soft fiber-reinforced bending actuators. *IEEE Transactions on Robotics*, 31, 778–789.
  23. Sanjuan, J. D., Castillo, A. D., Padilla, M. A., Quintero, M. C., & Rahman, M. H. (2020). Cable driven exoskeleton for upper-limb rehabilitation: A design review. *Robotics and Autonomous Systems*, 126, 103445.
  24. Chiaradia, D., Xiloyannis, M., Solazzi, M., Masia, L., & Frisoli, A. (2020). Chapter 4-rigid versus soft exoskeletons: interaction strategies for upper limb assistive technology. In L. Masia, S. Micera, M. Akay, & J. Pons (Eds.), *Converging clinical and engineering research on neurorehabilitation III. ICNR 2018. Biosystems & Biorobotics*. (Vol. 21). Cham: Springer.
  25. Xiloyannis, M., Chiaradia, D., Frisoli, A., & Masia, L. (2018). Characterisation of pressure distribution at the interface of a soft exosuit: Towards a more comfortable wear. In *International symposium on wearable robotics (WeRob 2018)* (vol. 22, pp. 35–38).
  26. Li, J. F., Zhao, P. B., & Zhang, L. Y. (2018). New type of self-adapting rehabilitation exoskeleton and gravity balance optimization. *Advanced Engineering Sciences*, 050, 263–270. in Chinese.
  27. Banala, S. K., Agrawal, S. K., Fattah, A., Krishnamoorthy, V., Hsu, W. L., Scholz, J., & Rudolph, K. (2006). Gravity-balancing leg orthosis and its performance evaluation. *IEEE Transactions on Robotics*, 22, 1228–1239.
  28. Li, H., Yu, H. L., Chen, Y. W., Tang, X. Y., Wang, D. J., Meng, Q. L., & Du, Q. (2022). Design of a minimally actuated lower limb exoskeleton with mechanical joint coupling. *Journal of Bionic Engineering*, 19, 370–389.
  29. Wu, Q. C., Wang, X. S., Wu, H. T., & Chen, B. (2017). Research on the gravity balance characteristics of an upper limb rehabilitation exoskeleton. *Robot*, 39, 81–8898. in Chinese.
  30. Wu, Q. C., & Wang, X. S. (2013). Design of a gravity balanced upper limb exoskeleton with Bowen cable actuators. *FACE Proceedings Volumes*, 46, 678–683. in Chinese.
  31. Puchinger, M., Kurup, N. B. R., & Gfoehler, M. (2019). Passive light-weight arm exoskeleton: possible applications. *Converging Clinical and Engineering Research on Neurorehabilitation III*, 21, 21–25.
  32. Hyun, D. J., Bae, K. H., Kim, K. J., Nam, S. K., & Lee, D. H. (2019). A light-weight passive upper arm assistive exoskeleton based on multi-linkage spring-energy dissipation mechanism for overhead tasks. *ScienceDirect Robotics and Autonomous Systems*, 122, 103309–103309.
  33. Mokhtari, M., Taghizadeh, M., & Mazare, M. (2021). Impedance control based on optimal adaptive high order super twisting sliding mode for a 7-DOF lower limb exoskeleton. *Meccanica*, 56, 535–548.
  34. Mokhtari, M., Taghizadeh, M., & Mazare, M. (2020). Hybrid adaptive robust control based on CPG and ZMP for a lower limb exoskeleton. *Robotica*, 39, 1–19.
  35. Mazare, M., & Taghizadeh, M. (2019). Geometric optimization of a delta type parallel robot using harmony search algorithm. *Robotica*, 37, 1494–1512.
  36. Neumann, D. (2010). *Kinesiology of the musculoskeletal system*. Mosby/Elsevier.
  37. Zhang, A. L. (2003). *The research on human upper limb kinetic analysis an simulation based on matlab*. Tianjin University of Science and Technology. in Chinese.
  38. Maxon group <https://www.maxongroup.com.cn/maxon/view/content/Product-Overview-Page>

**Publisher's Note** Springer Nature remains neutral with regard to jurisdictional claims in published maps and institutional affiliations.

Springer Nature or its licensor holds exclusive rights to this article under a publishing agreement with the author(s) or other rightsholder(s); author self-archiving of the accepted manuscript version of this article is solely governed by the terms of such publishing agreement and applicable law.